Ketolysis is Required for the Proper Development and Function of the Somatosensory Nervous System.

Jonathan Enders[1], Jarrid Jack[2], Sarah Thomas[1], Paige Lynch[1], Sarah Lasnier[1], Xin Cao[2], M Taylor Swanson[1,] Janelle M Ryals[1], John P. Thyfault[2,3,4], Patrycja Puchalska[5], Peter A. Crawford[5,6], and Douglas E Wright[1,4]

Departments of Anesthesiology[1], and Cell Biology and Physiology[2], Internal Medicine – Division of Endocrinology[3] and KU Diabetes Institute[4], University of Kansas Medical Center, Kansas City, KS, 66160.

Department of Medicine, Division of Molecular Medicine[5], Department of Molecular Biology, Biochemistry, and Biophysics[6], University of Minnesota, Minneapolis, MN, 55455.

For Correspondence: Douglas Wright

Department of Anesthesiology

University of Kansas Medical Center

Kansas City, KS 66160

Abstract

Ketogenic diets are emerging as protective interventions in preclinical and clinical models of somatosensory nervous system disorders. Additionally, dysregulation of succinyl-CoA 3-oxoacid CoA-transferase 1 (SCOT, encoded by *Oxct1*), the fate-committing enzyme in mitochondrial ketolysis, has recently been described in Friedreich's ataxia and amyotrophic lateral sclerosis. However, the contribution of ketone metabolism in the normal development and function of the somatosensory nervous system remains poorly characterized. We generated sensory neuron-specific, Advillin-Cre knockout of *Oxct1* (SNACKO) mice and characterized the structure and function of their somatosensory system. We used histological techniques to assess sensory neuronal populations, myelination, and innervation of the skin and spinal dorsal horn. We also examined cutaneous and proprioceptive sensory behaviors with the von Frey test, radiant heat assay, rotarod, and grid-walk tests. SNACKO mice exhibited myelination deficits, altered morphology of putative Aδ soma from the dorsal root ganglion, reduced cutaneous innervation, and abnormal innervation of the spinal dorsal horn compared to wildtype mice. Synapsin 1-Cre-driven knockout of *Oxct1* confirmed deficits in epidermal innervation following a loss of ketone oxidation. Loss of peripheral axonal ketolysis was further associated with proprioceptive deficits, yet SNACKO mice did not exhibit drastically altered cutaneous mechanical and thermal thresholds. Knockout of *Oxct1* in peripheral sensory neurons resulted in histological abnormalities and severe proprioceptive deficits in mice. We conclude that ketone metabolism is essential for the development of the somatosensory nervous system. These findings

also suggest that decreased ketone oxidation in the somatosensory nervous system may explain the neurological symptoms of Friedreich's ataxia.

Introduction

Ketolysis—the catabolism of β-hydroxybutyrate (β-HB) and acetoacetate for fuel—is known to contribute to the development and health of the nervous system. Ketone utilization is highest during neonatal periods, with β-HB uptake and activity of β-HB dehydrogenase 1 (BDH1) decreasing throughout development and into adulthood [1-3]. Acetoacetate prevents hippocampal lesions caused by inhibition of glycolysis in Wistar rats and increased adenosine triphosphate (ATP) production [4]. Likewise, β-HB protected from neuronal damage in albino rats and supported synaptic function following glycolytic inhibition in hippocampal slices from rats postnatal day 30 and earlier [5]. In disease states, ketogenic diets are neuroprotective in pediatric epilepsy [6, 7], and their use has led to improvements in Alzheimer's disease, cognitive impairment [8], and migraine [9, 10]. Together, these findings highlight the importance of metabolic plasticity between glycolysis and ketolysis in the developing and diseased central nervous system.

Little is known about ketone metabolism's contribution to somatosensory nervous system health. Ketone bodies are brought into peripheral tissues by the monocarboxylate transporters [11], after which they are utilized for metabolic and signaling functions [12, 13]. The obligate reaction during ketolysis is the addition of coenzyme A to acetoacetate catalyzed by succinyl-CoA 3-oxoacid CoA-transferase 1 (SCOT, encoded by *OXCT1*). *Oxct1* mRNA and SCOT protein expression are downregulated in mouse models of neurological diseases, including amyotrophic lateral sclerosis [14] and Friedreich's ataxia [15]. Ketone incorporation in lipid synthesis is

disrupted in the sciatic nerve of Trembler mouse models of Charcot-Marie-Tooth [16]. We previously published that ketone bodies support neurite outgrowth from dissociated dorsal root ganglia [17]. We also recently showed that ketone bodies are further protective in painful neuropathies by contributing to the detoxification of reactive dicarbonyls, such as methylglyoxal, that are elevated in diabetic neuropathy and directly cause neuronal dysfunction and pain [18]. Likewise, our works showed that a ketogenic diet supported the regeneration of lost intraepidermal nerve fibers in a model of peripheral diabetic neuropathy [19] and reversed pain-like behaviors in mouse models of type 1 diabetes [19] and prediabetes [17]. Additionally, sciatic nerve mitochondria from mice fed a ketogenic diet produce less reactive oxygen species [20]. Together, these prior findings suggest ketone metabolism likely plays a vital role in the protective effects of a ketogenic diet in the peripheral nerve.

To understand the contributions of ketone metabolism in the somatosensory nervous system, we used a Cre-lox system to generate a peripheral sensory neuron-specific knockout of *Oxct1,* referred to as sensory neuron, Advillin-Cre knockout of *Oxct1* (SNACKO) mice. We tested the hypothesis that ketone body metabolism or signaling was critical for somatosensory nervous system development by exploring potential changes in sensory neuronal phenotypes, peripheral axon integrity, and somatosensation in SNACKO mice. Our results suggest that ketone metabolism in sensory neurons is required for normal epidermal innervation and myelination of large peripheral axons. Sensory behaviors remain unchanged in SNACKO mice; however, these animals' response to intraplantar capsaicin was diminished and they demonstrated proprioceptive deficits. These findings provide important insight into

processes underlying ketone metabolism in the peripheral nerves. Moreover, these results provide an essential framework for understanding the potential therapeutic effects of a ketogenic diet on somatosensation and pain.

Materials and Methods

Animals and Breeding

All animal work was performed following review and approval by the Institutional Animal Care and Use Committee of Kansas University Medical Center. All mice were maintained on a 12:12 light: dark cycle in the Kansas University Medical Center animal research facility. In studies containing a ketogenic diet, mice were given *ad libitum* access to a ketogenic diet (TD.96355; Envigo, 90.5% fat, 9.2% protein, and 0.3% carbohydrate by kcal), which was replaced twice weekly. C57Bl6 mice carrying the *Oxct1*$^{flox/flox}$ allele and Synapsin-1 (*Syn1*)$^{+/Cre}$*Oxct1*$^{flox/flox}$ mice were generated previously [21]. Briefly, *Oxct1*$^{flox/flox}$ mice were crossed with *Advillin*$^{Cre/+}$ or *Syn1*$^{+/Cre}$ C57Bl6 mice (Jackson Laboratory, Bar Harbor, ME) to generate *Oxct1*$^{flox/+}$*Advillin*$^{Cre/+}$ and *Oxct1*$^{flox/+}$*Syn1*$^{+/Cre}$ mice. These mice were bred to *Oxct1*$^{flox/flox}$ mice, generating *Oxct1*$^{flox/flox}$*Advillin*$^{Cre/+}$ and *Oxct1*$^{flox/flox}$*Syn1*$^{+/Cre}$ mice. Male *Oxct1*$^{flox/flox}$*Advillin*$^{Cre/+}$ and *Oxct1*$^{flox/flox}$*Syn1*$^{+/Cre}$ mice were bred to *Oxct1*$^{flox/flox}$ females to produce Sensory Neuron, Advillin-Cre Knockout of *Oxct1* (SNACKO) mice and Syn1-Cre mice, respectively. Sensory neuronal knockout of *Oxct1* was confirmed by immunofluorescent microscopy of the dorsal root ganglion (DRG) (**Figure 1**). We primarily used SNACKO mice

throughout this work and included Syn1-Cre mice as evidence the effects observed were due to *Oxct1* knockout and not a Cre toxicity.

Blood Measurements

Fasting blood glucose was determined as described by Groover et al. [22]. Briefly, mice were fasted for 3 hours before drawing 20 µL blood from the tail vein by clipping off the tip of the tail, or the resulting scab in subsequent blood draws. We used Vaseline during the blood draw to avoid skin abrasion and improve scab healing. All standards and samples were mixed with molecular H_2O, $ZnSO_4$ (Sigma), and $Ba(OH)_2$ (Sigma) and centrifuged at 13000 rpm and 4 ^oC for 5 minutes. The supernatant was incubated for 30 minutes at 37 ^oC with color reagent (PGO capsule, Sigma; o-Dianisidine Dihydrochloride, Sigma; in molecular water). A plate reader (SpectraMax M5) determined the absorbance of standards and samples at 450 nm. Blood ketones were measured using a hand-held blood monitor and β-hydroxybutyrate blood ketone strips (β-Ketone blood test strips, Abbott Laboratories, Chicago, IL; Precision Xtra, Abbott Laboratories) after a 3-hour fast.

Cutaneous Sensory Behavior

Thresholds to mechanical and thermal stimulation were collected every 4 weeks in SNACKO mice starting at six weeks of age using Von Frey microfilaments and a Hargreaves Analgesiometer, respectively. Before data collection, mice were acclimated to testing areas for 30 minutes and the mesh table or thermal testing apparatus for 30 minutes on two occasions, separated by 24 hours. Finally, mice were acclimated to the

testing area, mesh table, and thermal testing apparatus for 30 minutes each before collecting data.

Different Von Frey monofilaments were applied for one second to the plantar surface of the hind paw following the “up-down” method [23]. Mice were observed for either a negative or a positive response, and the mechanical withdrawal threshold was calculated after five consecutive responses following the first positive response. Thermal sensitivity was determined by radiant heat assay using a thermal testing apparatus. A 4.2 V radiant heat source was applied to the plantar surface of the hind paw, and latency to withdrawal was recorded three times.

Mice were acclimated to a clear plastic cage without bedding for 5 minutes before capsaicin injection. Following intraplantar injection, mice were replaced in the cage. Capsaicin was diluted in sterile saline with 0.5% Tween 20 to a working concentration of 0.1 μg/μL and delivered by 20 μL subcutaneous injection to the right hind paw (20 μg). A blinded investigator then observed the mouse for 5 minutes following injection and recorded the total number of nocifensive events (licking, lifting, biting, guarding, etc.) the animal displayed and the total time spent engaged in nocifensive behavior.

Proprioceptive Sensory Behavior

Proprioception was measured at six weeks of age by a Rotorod test. Mice were acclimated to the rotarod via training sessions the day before data collection. On the day of data collection, mice were placed on the Rotarod treadmill (Med Associates, St Albans, VT). The rod of 32mm diameter, elevated 16 cm above the lab bench, was set

to ramp from 4 rpm to 40 rpm over a 300-sec duration as the mouse locomoted on the rod. Three trials were conducted with an intertrial interval of not less than 5 minutes, assessing an average latency to fall.

For the grid-walk test, mice were placed on a 35cm x 35cm wire mesh elevated 45cm above a lab bench with 1 cm^2 openings. During testing, mice were allowed to walk freely on the grid for 5 minutes while being filmed from grid level using a portable camera. Following testing, videos were reviewed by a blinded observer and analyzed for time spent walking, forepaw and hind paw slips, and total paw slips. Paw slips were defined as an extension of the limb through a wire opening to at least the ankle joint. Paw slips were normalized to time walking (slips/minute).

Tissue Processing and Immunofluorescent Microscopy

Mice were sacrificed by inhalation of isoflurane and decapitation. Dorsal root ganglia (DRG), footpads, and sciatic nerve were post-fixed overnight in 4% paraformaldehyde, Zamboni's fixative, and 2.5% glutaraldehyde with 2% paraformaldehyde, respectively. Fixed tissues were then rinsed with PBS. DRG, spinal cord, and footpad were soaked in 30% sucrose, rinsed, and then frozen in Optimal Cutting Temperature Compound (Sekura Tissue-Tek).

Dorsal Root Ganglia OXCT1 Detection and Sensory Neuronal Population Assessment

Eight-micron sections of L4-6 DRG were blocked for two hours in Superblock (ThermoFisher; Grand Island, NY), 1.5% Normal Donkey Serum, 0.5% Porcine Gelatin, and 0.5% Triton X-100 (Sigma) at room temperature. For OXCT1 detection, slides were incubated overnight with anti-post gene product 9.5 (PGP9.5) antibody (1:1500, UCHL1;

ProteinTech; Rosemont, IL). The next morning, slides were washed twice with PBS and stained with AlexaFluor488-tagged donkey-anti-rabbit secondary antibody (Molecular Probes, 1:1000) for one hour. Slides were washed twice with PBS, blocked with the same solution as before for at least two hours, and incubated with an anti-OXCT1 (1:250, AbCam) antibody overnight. Slides were then washed twice with PBS and incubated with AlexaFluor555-tagged donkey-anti-rabbit secondary antibody (Molecular Probes, 1:1000) for one hour. Slides were then washed twice with PBS and coverslipped. Fluorescent images were taken at 20x with a Nikon Eclipse Ti2 inverted microscope.

Slides were incubated overnight with anti-TrkA (goat, R&D Technologies, 1:250) and anti-NFH (rabbit, EMD Millipore, 1:1000) antibodies to assess various sensory neuronal populations. Slides were washed twice with phosphate-buffered saline for 5 minutes and incubated with Alexa Fluor 555-tagged donkey-anti-goat (Molecular Probes, 1:1000) and Alexa Fluor 647-tagged donkey-anti-rabbit (Molecular Probes, 1:1000) secondary antibodies for 1 hour. Slides were rinsed twice with PBS and incubated in freshly prepared Alexa Fluor 488-tagged IB4 (Invitrogen, 10µg/mL in 1M $CaCl_2$) for 10 minutes. Slides were rinsed twice in PBS and coverslipped before imaging with a Nikon Eclipse 90i microscope at 20x. At least five images were taken from each DRG. Neuron soma area and Feret diameter were determined by measurements with ImageJ software, and neurons were counted manually.

Intraepidermal Nerve Fiber Quantification

Thirty-micron sections of the footpad were blocked for two hours in Superblock (ThermoFisher; Grand Island, NY), 1.5% Normal Donkey Serum, 0.5% Porcine Gelatin,

and 0.5% Triton X-100 (Sigma) at room temperature. Slides were incubated overnight with rabbit α-PGP9.5 (1:1500, UCHL1; ProteinTech; Rosemont, IL) and goat α-TrkA (1:250; R&D Systems, Minneapolis, MN). Slides were incubated with Alexa Fluor 555 tagged donkey-α-rabbit secondary antibody (1:1000; Molecular Probes) and Alexa Fluor 488-tagged donkey-α-goat secondary antibody (1:1000; Molecular Probes) for one hour, then imaged with a Nikon Eclipse 90i microscope using a 20X objective. ImageJ software was used to measure the length of the dermal-epidermal junction. IENF was quantified as the number of fibers crossing that junction and expressed as the number of fibers per millimeter. Nine images were taken per slide, and the average IENF density for each mouse was used for statistical analyses.

Quantification of Myelination

Sciatic nerves were dissected out of 6-week-old WT and SNACKO mice, post-fixed in 2.5% glutaraldehyde and 2% paraformaldehyde overnight at 4 ^{o}C and rinsed with phosphate-buffered saline. Tissue was then embedded in paraffin blocks, semithin (1 µm) cross sections were cut by microtome, and sections were stained with toluidine blue before coverslipping. Brightfield images were taken at 30x with a Nikon Eclipse Ti2 inverted microscope. The “GRatio” plugin was used with ImageJ to randomly select and measure the area and perimeter of axons and their associated myelin from each image. Thin sections (70-85 µm) were cut with a DiATOME diamond knife, post-stained with uranyl acetate and lead citrate, and imaged with a JEOL JEM-1400 transmission electron microscope (TEM) at 100 kV. At least five images were taken of each sample at 1000x and 2000x. Dysmyelination was defined as invagination, separation from the axoplasm, and unraveling of the myelin (**Figure 4E-F**). These events were quantified as

a frequency of dysmyelinated axons among all myelinated axons completely captured in a field of view by a blinded observer. Remak bundle occupancy was quantified by counting the total number of unmyelinated fibers within Remak bundles completely captured in a field of view normalized to the number of Remak bundles within that view.

Quantification of Spinal Dorsal Horn Innervation

The lumbar enlargement of the spinal cord was dissected out of 6-week-old WT and SNACKO mice, post-fixed in 4% paraformaldehyde and soaked in 30% sucrose. 30 µm sections were blocked for two hours in Superblock, 1.5% Normal Donkey Serum, 0.5% Porcine Gelatin, and 0.5% Triton X-100 at room temperature. Sections were stained overnight with goat anti-TrkA antibody (1:250). Sections were washed with phosphate-buffered saline, stained with freshly prepared Alexa Fluor 488-tagged IB4 (10µg/mL in 1M $CaCl_2$) for 10 minutes, washed again, and stained with Alexa Fluor 555-tagged donkey-α-goat secondary antibody (Molecular Probes, 1:1000) for 1 hour. Sections were coverslipped and imaged with a Nikon Eclipse Ti2 inverted microscope at 10x. The area of TrkA-positive innervation of lamina I and IB4-positive innervation of lamina IIo were quantified by ImageJ. A blinded observer manually counted the number of TrkA-positive projections extending through lamina II into lamina III or deeper. At least five images of the dorsal horn of the spinal cord were taken for each mouse, and the average $TrkA^+$ and $IB4^+$ areas and the number of deeper $TrkA^+$-projections were used for statistical analysis.

Statistical Analyses

All statistical analyses were performed using R version 3.6.2 and packages “Rmisc”, “car”, and “ggpubr”. All analyses for which data were collected over time were performed using a mixed-model analysis of variance (ANOVA) with repeated measures. All other analyses were performed using a two-way ANOVA or Student’s t-test, as appropriate. As indicated, data were analyzed posthoc by pairwise t-test or Tukey’s Honest Significant Difference (HSD). Data are presented as mean +/- standard error of the mean in bar and line charts or as median with interquartile range in violin plots. Type I error rate was set at 0.05 except where noted due to a Bonferroni correction for multiple comparisons.

Results

SNACKO mice have nearly complete ablation of SCOT in dorsal root ganglia neurons.

We confirmed the loss of *Oxct1* in sensory neurons using immunofluorescent microscopy. Neuronal soma in the dorsal root ganglia (DRG) were stained positively for SCOT in $Oxct^{flox/flox}Adv^{+/+}$ mice (wildtype mice, hereafter) (**Figure 1**). SNACKO mice were negative for SCOT staining in the neuronal soma of the DRG, indicating the absence of the enzyme from peripheral sensory neurons.

Sensory neuronal knockout of Oxct1 has minimal effect on whole-body metabolism.

Neuronal knockout of *Oxct1* has been associated with dysregulation of blood glucose and serum ketones [21]. Given the effect of metabolic syndrome and diabetes on peripheral nervous system health, we characterized metabolic markers in wildtype and SNACKO mice. SNACKO mice were modestly but significantly heavier than wildtype mice (**Figure 2A**; N-way mixed-model ANOVA with repeated measures, genotype: p =

0.00176). We detected a sex difference in the effect of genotype (genotype-sex interaction: $p = 7.28e^{-5}$). SNACKO males trended toward reduced body weight compared to their wildtype littermates (**Figure 2B**; Tukey's *post hoc*, p = 0.055), while SNACKO females were significantly heavier than their wildtype littermates (**Figure 2C**; Tukey's *post hoc*, p = 0.0041). We did not detect sex differences in fasting blood glucose or circulating ketones and thus pooled and reanalyzed the data. There was no significant difference in fasting blood glucose between chow-fed wildtype and SNACKO mice (**Figure 2D**; N-way mixed-model ANOVA with repeated measures, genotype: p = 0.103, genotype-time interaction: p = 0.508), nor were there differences in the abundance of circulating β-HB (**Figure 2E**; N-way mixed-model ANOVA with repeated measures, genotype: p = 0.506, genotype-time interaction: p = 0.701). To asses the consequences of peripheral nerve knockout of SCOT on circulating ketone levels, six week-old wildtype and SNACKO mice were fed a ketogenic diet for one week. Consumption of a ketogenic diet caused an increase in circulating β-HB in both genotypes (**Figure 2F**; N-way ANOVA, genotype: $p = 2.06e^{-6}$). Additionally, there was a strong but statistically insignificant trend toward an effect of genotype (p = 0.0679) and genotype-diet interaction (p = 0.0775). For all measures of fasting blood glucose and circulating β-HB, mice fasted for 3 hours.

SNACKO mice have larger TrkA$^+$ NF-H$^+$ Dorsal Root Ganglia Soma than wildtypes.

We harvested DRG from wildtype and SNACKO mice to assess changes in peptidergic (TrkA$^+$), non-peptidergic (IB4$^+$), and myelinated (neurofilament heavy, NF-H$^+$) sensory neuron populations (**Figure 3A**). We performed a Bonferroni correction to account for multiple comparisons in analyzing these populations and set our α-level at 0.005. We

detected no significant differences in the area (Student's t-test, p = 0.332) or diameter (Student's t-test, p = 0.4761) of all TrkA$^+$ soma (**Figure 3B**). Likewise, no changes were present in area (Student's t-test, p = 0.9375) or diameter (Student's t-test, p = 0.7313) in IB4$^+$ neurons (**Figure 3C**). We detected a statistically significant increase in NF-H$^+$ soma area (Student's t-test, p = 0.002919) but not diameter (Student's t-test, p = 0.01043) in SNACKO mice (**Figure 3D**). Both area (Student's t-test, p = 0.001008) and diameter (Student's t-test, p = 0.0004735) were increased in TrkA$^+$ NF-H$^+$ DRG soma from SNACKO mice (**Figure 3E**); however, no differences were detected in the area (Student's t-test, p = 0.6901) or diameter (Student's t-test, p = 0.5898) of TrkA$^+$ NF-H$^-$ soma (**Figure 3F**).

Myelination aberrations are present in SNACKO mice.

We harvested sciatic nerves from 6-week-old SNACKO and wildtype mice and stained 1µm nerve sections in cross-section with toluidine blue to visualize myelin (**Figure 4A-B**). The analysis revealed an abundance of small, hypermyelinated axons in SNACKO mice (**Figure 4B**). These hypermyelinated axons were clearly reflected in g-ratio based on myelin and axon area (Student's t-test, p = 0.009114) and circumference (Student's t-test, p = 0.02255) measurements (**Figure 4C-D**). An analysis by transmission electron microscopy similarly revealed an increased in abnormal myelinated axons in SNACKO mice compared to wildtypes (**Figure 4E-G**; Student's t-test, p = 0.01713). We also detected differences in the number of unmyelinated axons occupying Remak bundles. Remak bundles from wildtype mice contained significantly more C-fibers than SNACKO mice (**Figure 4E-F, H**; Student's t-test, p = 0.0399).

SNACKO mice have largely unaltered mechanical and thermal sensitivity.

We observed no significant differences in mechanical withdrawal threshold between wildtype and SNACKO mice (**Figure 5A**; N-way mixed-models ANOVA with repeated-measures, genotype: $p = 0.645$, genotype-time interaction: $p = 0.38$). Likewise, cold sensitivity was similar between both genotypes as determined by cold plate assay (**Figure 5C**; Student's t-test, $p = 0.2535$). SNACKO mice trended toward increased sensitivity to radiant heat (**Figure 5B**; N-way mixed-models ANOVA with repeated-measures, genotype: $p = 0.0775$, genotype-time interaction: $p = 0.0578$).

Surprisingly, SNACKO mice displayed an attenuated nociceptive response to intraplantar capsaicin injection compared to wildtype mice. Capsaicin injection significantly increased the number of nociceptive events (licking, biting, shaking, etc.) (**Figure 5D**; 2-way ANOVA, genotype: $p = 0.023$, injection: $p = 1.32e^{-7}$, genotype-injection interaction: $p = 0.00502$) and time engaged in nociceptive behavior towards the injected paw (**Figure 5E**; 2-way ANOVA, genotype: $p = 0.05$, injection: $p = 2.5e^{-5}$, genotype-injection interaction: $p = 0.0236$) in both genotypes. SNACKO mice receiving capsaicin injection engaged in fewer nociceptive events (Tukey's *post hoc*, SNACKO-capsaicin and wildtype-capsaicin, $p = 0.00125$) and spent less time engaged in nociceptive behaviors (Tukey's *post hoc*, SNACKO-capsaicin, and wildtype-capsaicin, $p = 0.00987$) than wildtype mice receiving capsaicin.

SNACKO mice have decreased epidermal innervation.

To assess whether absent ketolysis in peripheral neurons affected epidermal innervation, we harvested footpads from wildtype and SNACKO mice at 6 weeks of age and used PGP9.5 and tyrosine receptor kinase A (TrkA) antibodies to visualize axonal populations (**Figure 6A**). Using these antibodies, $PGP9.5^{+}TrkA^{+}$ axons were considered

peptidergic, while PGP9.5^{+}TrkA^{-} axons were counted as nonpeptidergic epidermal axons. SNACKO mice had a significantly reduced overall intraepidermal nerve fiber (IENF) density (**Figure 6B**; Student's t-test, p = 0.0042), reduced peptidergic IENF density (**Figure 6C**; Student's t-test, p = 0.00279), and reduced nonpeptidergic IENF density (**Figure 6D**, Student's t-test, p = 0.014). SNACKO mice had a slight but statistically significant increased ratio of nonpeptidergic to peptidergic IENFs compared to wildtype mice (**Figure 6E**; Student's t-test, p = 0.0455).

We obtained footpad tissue from an alternative mouse line in which Oxct1 was knocked out using a pan-neuronal promoter (*Syn1*$^{+/Cre}$*Oxct1*$^{flox/flox}$ mice, hereafter Syn1-Cre). Comparisons of epidermal innervation of 26-30-week-old wildtype, SNACKO, and pan-neuronal (Syn1-Cre) mice (**Figure 6F)** revealed significantly reduced IENF density in both SNACKO and Syn1-Cre mice (**Figure 6G**; 1-way ANOVA, genotype: p = 9.5e^{-5}; Tukey's *post hoc*, wildtype-SNACKO: p = 0.000342, wildtype-Syn1-Cre: p = 0.000106). Both SNACKO and Syn1-Cre mice had significantly fewer PGP9.5^{+}TrkA^{+} peptidergic fibers compared to wildtype mice (**Figure 6H**, 1-way ANOVA, genotype: p = 0.00362; Tukey's *post hoc*, wildtype-SNACKO: p = 0.011, wildtype-Syn1-Cre: p = 0.0039). Only Syn1-Cre had significantly reduced TrkA- non-peptidergic IENF density compared to wildtype mice (**Figure 6I**, 1-way ANOVA, genotype: p = 0.0427; Tukey's *post hoc*, wildtype-SNACKO: p = 0.0847, wildtype-Syn1-Cre: p = 0.0471).

SNACKO mice have abnormal afferent innervation of the spinal dorsal horn.

We assessed the effect of the absence of sensory axonal ketolysis on sensory axon terminations in the dorsal horn of the lumbar spinal cord (**Figure 7A**). We detected no

difference in the distribution TrkA$^+$ fibers in the superficial Rexed lamina I between SNACKO and wildtype mice (**Figure 7B**; Student's t-test, p = 0.8394). Likewise, we detected no difference in IB4$^+$ innervation of lamina IIo (**Figure 7C**; Student's t-test, p = 0.8207). We did, however, notice more TrkA$^+$ projections extending into the deeper lamina of the dorsal horn in SNACKO mice compared to WT (**Figure 7A**, *white arrow heads*). Following a Bonferroni corrections for multiple comparisons (n comparisons = 3), counts of the number of TrkA$^+$ axons extending to deeper lamina reached statistical significance (**Figure 7D**, Student's t-test, p = 0.01551).

SNACKO mice exhibit impaired proprioception and coordination.

We tested gross coordination and balance in male and female SNACKO and wildtype mice using a Rotorod. We detected no significant differences in latency to fall between SNACKO and wildtype mice (**Figure 8A**, 2-way ANOVA, genotype: p = 0.549, sex: p = 0.0696, genotype-sex interaction: p = 0.3092). As an additional measure of proprioception, mice were subjected to a grid-walk test. During a timed grid-walk, SNACKO mice spent less time walking on the grid than wildtype mice (**Figure 8B** 2-way ANOVA, genotype: p = 2.43e^{-5}, sex: p = 0.639, genotype-sex interaction: p = 0.909). When normalized to the amount of time walking, SNACKO mice also exhibited an increased number of total paw slips (**Figure 8C**, 2-way ANOVA, genotype: p = 1.03e^{-10}, sex: p = 0.401, genotype-sex interaction: p = 0.234), which was attributed to impaired coordination of both the forepaw (**Figure 8D**, 2-way ANOVA, genotype: p = 2.79e^{-10}, sex: p = 0.373, genotype-sex interaction: p = 0.122) and hind paw (**Figure 8E**, 2-way ANOVA, genotype: p = 4.51e^{-8}, sex: p = 0.657, genotype-sex interaction: p = 0.783).

Discussion

There is mounting evidence that ketone utilization is protective [17, 24, 25] and, in some cases, promotes regeneration [19] in the somatosensory nervous system of rodent models of chronic pain and neuropathy. SCOT is a mitochondrial enzyme expressed in peripheral tissues and required for ketolysis, catalyzing the conversion of acetoacetate and succinyl-CoA to acetoacetyl-CoA and succinate. *Oxct1* mRNA and SCOT protein are downregulated in rodent models of amyotrophic lateral sclerosis [14] and Friedreich's ataxia [15], as well as in fibroblasts from Friedreich's ataxia patients [15]. The contribution of impaired ketone metabolism in these diseases is unclear. In addition, relatively little is known about the importance of ketone metabolism in the normal development and maintenance of the somatosensory nervous system.

Our studies demonstrate that sensory neuron-specific knockout of *Oxct1* leads to pathological changes in the somatosensory nervous system. SNACKO mice have significantly fewer IENFs in the glabrous skin of the hindpaw. IENFs are comprised of unmyelinated C-fibers, which, in mice, can be subdivided into developmentally distinct peptidergic and non-peptidergic axon populations [26], marked by the presence or absence of tropomyosin receptor kinase A (TrkA) and positive staining for neuropeptides or the lectin IB4, respectively. These epidermal fibers degenerate at different rates during diabetes [27] and following nerve injury [28], and changes in the proportion of "non-peptidergic" to "peptidergic" fibers have been associated with abnormal sensation in obese mice [22]. Six-week-old SNACKO mice exhibited reduced cutaneous innervation by both "peptidergic" (PGP9.5^{+} TrkA^{+},) and "non-peptidergic" (PGP9.5^{+} TrkA^{-},) fibers. While SNACKO mice had fewer IENFs than wildtype mice, we

did not detect any differences in “peptidergic” (TrkA^{+} NF-H^{-}) or “non-peptidergic" (IB4^{+}) soma in the DRG between genotypes. However, the consistent and significant loss of epidermal axons in SNACKO and Syn1-Cre Oxct1 mice suggests that axonal ketone oxidation is critical to developing and maintaining a full complement of axonal terminations in the epidermis.

Loss of IENF density is a hallmark of small-fiber neuropathy and is observed in various conditions associated with chronic pain in both humans [29-32] and rodents [17, 19, 27, 33]. Prior work from our laboratory has demonstrated that sensory abnormalities usually precede these anatomic changes [17, 27]. While SNACKO mice exhibit lower IENF density than wildtype mice, their mechanical and thermal thresholds remained largely unchanged. SNACKO mice demonstrated no significant changes in responsiveness to mechanical or cold stimuli. There was a strong trend toward increased responsiveness to radiant heat in SNACKO mice that was lost with age, though this failed to reach statistical significance. The discrepancy between reduced epidermal innervation but normal sensory thresholds is consistent with the view that these two aspects are not always linked [17, 34, 35]. Surprisingly, following capsaicin injection, SNACKO mice exhibited fewer nocifensive behaviors than their wildtype littermates. Thus, our results suggest that deficiencies in ketone oxidation in peripheral sensory neurons may be more important in responses to noxious chemicals like capsaicin.

In addition to altered cutaneous innervation, loss of *Oxct1* was associated with increased sizes of myelinated, peptidergic DRG soma. This neuronal population fits the PEP2 classification (TrkA^{+} NF-H^{+}), representing nociceptive Aδ fibers, described by Usoskin et. al. [36]. However, single-cell quantitative polymerase chain reaction and

electrophysiological profiling of the DRG suggests that TrkA$^+$ NF-H$^+$ soma represent A-fiber high-threshold mechanoreceptors (HTMRs) or another population of A-fibers [37]. Adelman and colleagues describe this other population as large dynamic range neurons, though their characteristics are consistent with low-threshold mechanoreceptors (LTMRs)[37]. Our analysis was insufficient to determine whether the increased size in TrkA$^+$ NF-H$^+$ soma represents a change in either HTMRs or LTMRs, as SNACKO mice exhibited no changes in mechanical sensitivity. Electrophysiological profiling of these mice is thus required to confirm the functional identity of this population, though both studies above indicate these neurons likely represent Aδ sensory neurons.

The changes in TrkA$^+$ NF-H$^+$ neurons were accompanied by abnormal myelination of axons in the sciatic nerve of SNACKO mice. SNACKO mice demonstrated a clear tail of decreased g-ratio in axons smaller than 10 μm^2, indicating that these smaller fibers are hypermyelinated. This area correlates to ~1.8 μm diameter axons, well within the fiber diameters of putative Aδ neurons. It is unclear why Aδ neurons would be uniquely susceptible during development without ketone oxidation compared to unaffected populations. Aδ HTMRs are critically reliant on nerve growth factor (NGF)-TrkA signaling between postnatal day 0 and 14 [38], and advillin expression—and thus, *Oxct1* knockout in our animals—is present in the DRG by postnatal day 0 [39]. Ketone metabolism may dampen the NGF-TrkA signaling axis. This explanation is consistent with somal and myelination changes in an Aδ population, as NGF signaling promotes myelination in the peripheral nervous system [40].

It is also possible that decreased axonal ketone oxidation increases the availability of ketone bodies for myelin biosynthesis. Radiolabeling studies demonstrate the preferential use of ketone-derived acetyl groups in myelin sterol biosynthesis in the rat brain [41] and mouse sciatic nerve [16] over those derived from glycolysis. As sensory axons no longer consume ketones as fuel in these mice, myelinating Schwann cells may instead shuttle β-HB and acetoacetate into myelin lipid synthesis, explaining the hypermyelination phenotype. While chow-fed SNACKO mice do not exhibit elevated circulating β-HB levels compared to wildtype mice, there was a strong trend toward increased circulating β-HB levels in ketogenic diet-fed SNACKO mice compared to wildtype (**Figure 2**). This indicates there is no change in basal ketone utilization even in the absence of axonal ketolysis, and these data are consistent with alternative avenues of ketone utilization, including incorporation into myelin cholesterol. Further, the trend toward increased circulating blood ketones in SNACKO mice during nutritional ketosis suggests SNACKO mice lose SCOT function in the somatosensory nervous system.

In addition to sensory changes, myelination pathology, and axon deficiencies and abnormalities, loss of *Oxct1* in sensory neurons led to gait dysfunction. An analysis of grid-walk revealed significant disruptions to fore- and hind-limb proprioception in the SNACKO mice. Collectively this pattern of sensory deficits is relevant, as a recent study has reported that *Oxct1* expression is downregulated in both mouse models and patient samples of Friedreich's ataxia [15]. The neurological symptoms of Friedreich's ataxia include a loss of cutaneous sensation, altered gait, fatigue, and worsening balance and proprioception [42-44]. Mouse models of Friedreich's ataxia likewise demonstrate altered gait and poor proprioception [45, 46]. In this new study, mutant frataxin leads to

increased ubiquitination of OXCT1, leading to its degradation and severely impaired ketone metabolism in fibroblasts and skeletal muscle [15]. As our analysis of SNACKO mice was in relatively young mice, it will be important to determine the breadth of sensory changes as these mice age and how these changes correlate with the breadth of symptoms in patients with Friedreich's ataxia [42, 44]. Our work suggests that impaired ketone metabolism in peripheral sensory neurons can mimic the neurological deficits of Friedreich's ataxia and supports the model in which mutant frataxin mediated downregulates SCOT and ketolysis, contributing to the clinical symptoms of this disease.

The importance of proper energy metabolism in the function of the somatosensory nervous system is emerging rapidly. Deficiencies in ketolysis have been recently revealed in neurodegenerative diseases, including Friedreich's ataxia and amyotrophic lateral sclerosis [14, 15]. Meanwhile, ketogenic diets are being studied in various neuropathies [17-19, 24, 25, 47, 48]. Our findings on the loss of *Oxct1* and SCOT in peripheral neurons provide new information towards our understanding of ketone oxidation for developing and maintaining the peripheral sensory nervous system. Overall, these findings suggest that ketone oxidation is essential for the normal development of sensory axons, highlights the deleterious effects of deficient ketone metabolism during development and provides a new link to possible mechanisms leading to sensory dysfunction in patients with Friedreich's ataxia.

Acknowledgments

This work was supported by NIH grants R01 NS043314 (DEW), R01 AG069781 (PAC and JPT), R01 DK091538 (PAC), the Kansas Institutional Development Award (IDeA) P20 GM103418, Kansas University Training Program in Neurological and Rehabilitation Sciences NIH T32HD057850 (JE), Translating Obesity, Metabolic Dysfunction, and Comorbid Disease States NIH T32DK128770 (ST), the Kansas IDDRC P30HD00228, and University of Minnesota Institute for Diabetes, Obesity, and Metabolism.

Conflict of interest

P.A.C. has consulted for Pfizer, Inc., Abbott Laboratories, and Jansen Research & Development. The other authors declare no competing financial interests.

Author contributions

JE and DEW designed the research study; JE, JMR, MTS, PL, JJ, ST, SL, and XC performed the experiments; JE and DEW analyzed the data; all authors contributed to the manuscript.

Bibliography

1. Kraus, H., S. Schlenker, and D. Schwedesky, *Developmental Changes of Cerebral Ketone Body Utilization in Human Infants.* Biological Chemistry, 1974. **355**(1): p. 164-170.
2. Bilger, A. and A. Nehlig, *Quantitative histochemical changes in enzymes involved in energy metabolism in the rat brain during postnatal development. II. Glucose-6-phosphate dehydrogenase and β-hydroxybutyrate dehydrogenase.* International Journal of Developmental Neuroscience, 1992. **10**(2): p. 143-152.
3. Nehlig, A., S. Boyet, and A.P. de Vasconcelos, *Autoradiographic measurement of local cerebral β-hydroxybutyrate uptake in the rat during postnatal development.* Neuroscience, 1991. **40**(3): p. 871-878.
4. Massieu, L., et al., *Acetoacetate protects hippocampal neurons against glutamate-mediated neuronal damage during glycolysis inhibition.* Neuroscience, 2003. **120**(2): p. 365-378.
5. Izumi, Y., et al., *beta-Hydroxybutyrate fuels synaptic function during development. Histological and physiological evidence in rat hippocampal slices.* The Journal of clinical investigation, 1998. **101**(5): p. 1121-1132.
6. Sourbron, J., et al., *Ketogenic diet for the treatment of pediatric epilepsy: review and meta-analysis.* Child's Nervous System, 2020. **36**(6): p. 1099-1109.
7. Henderson, C.B., et al., *Efficacy of the ketogenic diet as a treatment option for epilepsy: meta-analysis.* Journal of child neurology, 2006. **21**(3): p. 193-198.
8. Taylor, M.K., et al., *Feasibility and efficacy data from a ketogenic diet intervention in Alzheimer's disease.* Alzheimer's & Dementia: Translational Research & Clinical Interventions, 2018. **4**: p. 28-36.
9. Bongiovanni, D., et al., *Effectiveness of ketogenic diet in treatment of patients with refractory chronic migraine.* Neurological Sciences, 2021. **42**(9): p. 3865-3870.
10. Di Lorenzo, C., et al., *A ketogenic diet normalizes interictal cortical but not subcortical responsivity in migraineurs.* BMC neurology, 2019. **19**(1): p. 1-9.
11. Hugo, S.E., et al., *A monocarboxylate transporter required for hepatocyte secretion of ketone bodies during fasting.* Genes Dev, 2012. **26**(3): p. 282-93.
12. Puchalska, P. and P.A. Crawford, *Multi-dimensional Roles of Ketone Bodies in Fuel Metabolism, Signaling, and Therapeutics.* Cell metabolism, 2017. **25**(2): p. 262-284.
13. Puchalska, P. and P.A. Crawford, *Metabolic and Signaling Roles of Ketone Bodies in Health and Disease.* Annual Review of Nutrition, 2021. **41**(1): p. 49-77.
14. Szelechowski, M., et al., *Metabolic Reprogramming in Amyotrophic Lateral Sclerosis.* Scientific Reports, 2018. **8**(1): p. 3953.
15. Dong, Y.N., et al., *Frataxin controls ketone body metabolism through regulation of OXCT1.* PNAS Nexus, 2022.
16. Clouet, P.M. and J.-M. Bourre, *Ketone Body Utilization for Lipid Synthesis in the Murine Sciatic Nerve: Alterations in the Dysmyelinating Trembler Mutant.* Journal of Neurochemistry, 1988. **50**(5): p. 1494-1497.

17. Cooper, M.A., et al., *A ketogenic diet reduces metabolic syndrome-induced allodynia and promotes peripheral nerve growth in mice.* Experimental Neurology, 2018. **306**: p. 149-157.
18. Enders, J., et al., *A ketogenic diet prevents methylglyoxal-evoked nociception by scavenging methylglyoxal.* The Journal of Pain, 2022. **23**(5): p. 24.
19. Enders, J., et al., *A ketogenic diet reduces mechanical allodynia and improves epidermal innervation in diabetic mice.* Pain, 2021.
20. Cooper, M.A., et al., *Reduced mitochondrial reactive oxygen species production in peripheral nerves of mice fed a ketogenic diet.* Experimental physiology, 2018. **103**(9): p. 1206-1212.
21. Cotter, D.G., et al., *Successful adaptation to ketosis by mice with tissue-specific deficiency of ketone body oxidation.* American Journal of Physiology-Endocrinology and Metabolism, 2013. **304**(4): p. E363-E374.
22. Groover, A.L., et al., *Exercise-mediated improvements in painful neuropathy associated with prediabetes in mice.* PAIN®, 2013. **154**(12): p. 2658-2667.
23. Chaplan, S.R., et al., *Quantitative assessment of tactile allodynia in the rat paw.* J Neurosci Methods, 1994. **53**(1): p. 55-63.
24. Ruskin, D.N., et al., *Ketogenic diet effects on inflammatory allodynia and ongoing pain in rodents.* Scientific Reports, 2021. **11**(1): p. 1-8.
25. Zhong, S., et al., *Ketogenic diet prevents paclitaxel-induced neuropathic nociception through activation of PPARγ signalling pathway and inhibition of neuroinflammation in rat dorsal root ganglion.* European Journal of Neuroscience, 2021. **54**(4): p. 5341-5356.
26. Molliver, D., et al., *IB4-binding DRG neurons switch from NGF to GDNF dependence in early postnatal life.* Neuron, 1997. **19**(4): p. 849-861.
27. Johnson, M.S., J.M. Ryals, and D.E. Wright, *Early loss of peptidergic intraepidermal nerve fibers in an STZ-induced mouse model of insensate diabetic neuropathy.* Pain, 2008. **140**(1): p. 35-47.
28. Wang, T., et al., *Phenotypic Switching of Nonpeptidergic Cutaneous Sensory Neurons following Peripheral Nerve Injury.* PLOS ONE, 2011. **6**(12): p. e28908.
29. Chien, Y.-L., et al., *Small fiber pathology in autism and clinical implications.* Neurology, 2020. **95**(19): p. e2697-e2706.
30. Cheng, H.T., et al., *Increased axonal regeneration and swellings in intraepidermal nerve fibers characterize painful phenotypes of diabetic neuropathy.* The journal of pain, 2013. **14**(9): p. 941-947.
31. Bednarik, J., et al., *Etiology of small-fiber neuropathy.* Journal of the Peripheral Nervous System, 2009. **14**(3): p. 177-183.
32. Kluding, P.M., et al., *The effect of exercise on neuropathic symptoms, nerve function, and cutaneous innervation in people with diabetic peripheral neuropathy.* Journal of Diabetes and its Complications, 2012. **26**(5): p. 424-429.
33. Jack, M.M., J.M. Ryals, and D.E. Wright, *Protection from diabetes-induced peripheral sensory neuropathy — A role for elevated glyoxalase I?* Experimental Neurology, 2012. **234**(1): p. 62-69.
34. Wright, D.E., et al., *Selective changes in nocifensive behavior despite normal cutaneous axon innervation in leptin receptor–null mutant (db/db) mice.* Journal of the Peripheral Nervous System, 2007. **12**(4): p. 250-261.

35. Tierney, J.A., et al., *High-fat diet causes mechanical allodynia in the absence of injury or diabetic pathology.* Scientific reports, 2022. **12**(1): p. 1-13.
36. Usoskin, D., et al., *Unbiased classification of sensory neuron types by large-scale single-cell RNA sequencing.* Nature Neuroscience, 2015. **18**(1): p. 145-153.
37. Adelman, P.C., et al., *Single-cell q-PCR derived expression profiles of identified sensory neurons.* Molecular Pain, 2019. **15**: p. 1744806919884496.
38. Lewin, G.R., A.M. Ritter, and L. Mendell, *On the role of nerve growth factor in the development of myelinated nociceptors.* Journal of Neuroscience, 1992. **12**(5): p. 1896-1905.
39. Zurborg, S., et al., *Generation and characterization of an Advillin-Cre driver mouse line.* Molecular pain, 2011. **7**: p. 1744-8069-7-66.
40. Chan, J.R., et al., *NGF Controls Axonal Receptivity to Myelination by Schwann Cells or Oligodendrocytes.* Neuron, 2004. **43**(2): p. 183-191.
41. Koper, J.W., M. Lopes-Cardozo, and L.M.G. Van Golde, *Preferential utilization of ketone bodies for the synthesis of myelin cholesterol in vivo.* Biochimica et Biophysica Acta (BBA) - Lipids and Lipid Metabolism, 1981. **666**(3): p. 411-417.
42. Creigh, P.D., et al., *Measuring peripheral nerve involvement in Friedreich's ataxia.* Annals of clinical and translational neurology, 2019. **6**(9): p. 1718-1727.
43. Delatycki, M.B., L.A. Corben, and B.L. Maria, *Clinical Features of Friedreich Ataxia.* Journal of Child Neurology, 2012. **27**(9): p. 1133-1137.
44. Nolano, M., et al., *Small fibers involvement in Friedreich's ataxia.* Annals of Neurology, 2001. **50**(1): p. 17-25.
45. Gérard, C., et al., *A promising mouse model for Friedreich Ataxia progressing like human patients.* Behavioural Brain Research, 2023. **436**: p. 114107.
46. Piguet, F., et al., *Rapid and Complete Reversal of Sensory Ataxia by Gene Therapy in a Novel Model of Friedreich Ataxia.* Molecular Therapy, 2018. **26**(8): p. 1940-1952.
47. Field, R., F. Pourkazemi, and K. Rooney, *Effects of a Low-Carbohydrate Ketogenic Diet on Reported Pain, Blood Biomarkers and Quality of Life in Patients with Chronic Pain: A Pilot Randomized Clinical Trial.* Pain Medicine, 2022. **23**(2): p. 326-338.
48. Ruskin, D.N., M. Kawamura Jr, and S.A. Masino, *Reduced pain and inflammation in juvenile and adult rats fed a ketogenic diet.* PloS one, 2009. **4**(12): p. e8349.

Figure Legends

Figure 1. SNACKO mice lack expression of *Oxct1* in the dorsal root ganglia. Representative micrographs of dorsal root ganglia (DRG) stained from wildtype (WT) and Sensory nerve, Advillin-Cre Knockout of *Oxct1* (SNACKO) mice. Scale bar is 100 μm.

Figure 2. SNACKO mice do not exhibit drastic changes in systemic metabolic markers. (A) The body weight of wildtype and SNACKO mice varied by both genotype and genotype-sex interaction. Male SNACKO mice were largely not different from wildtype mice, though there was a trend toward decreased size (B). Female SNACKO mice, however, had consistently heavier body weight than their littermate, wildtype controls (C). Fasting blood glucose (FBG) (D) and circulating β-hydroxybutyrate (E) were unchanged between SNACKO and wildtype mice. (F) On consumption of a ketogenic diet for one week, circulating β-HB was significantly increased in both genotypes, and there was a trend toward further increased circulating β-HB in SNACKO mice. (D-E) Mice were fasted for three hours before each measure of FBG and β-hydroxybutyrate. N-way, mixed-models ANOVA, ** indicates effect of genotype: $p < 0.01$, ††† indicates effect of genotype-sex interaction: $p < 0.005$. (F) N-way ANOVA, *** indicates effect of genotype: $p < 0.005$.

Figure 3. Loss of *Oxct1* during development alters the soma morphology of small, myelinated peptidergic sensory neurons. (A) Representative micrographs of wildtype

and SNACKO DRG stained for tropomyosin receptor kinase A (TrkA, red), isolectin B4 (IB4, green), and neurofilament heavy chain (NF-H). Scale bar represents 50 µm. There were no differences in the area or diameter of $TrkA^+$ (B) or $IB4^+$ (C) soma. There was a significant increase in the area, but not diameter, of $NF\text{-}H^+$ soma in SNACKO mice (D). SNACKO mice also demonstrated in increased area and diameter of $TrkA^+$ $NF\text{-}H^+$ soma (E), yet there were no differences in the size of $TrkA^+$ $NF\text{-}H^-$ soma (F). Student's t-test with a Bonferroni correction, * indicates $p < 0.005$, ** indicates $p < 0.001$, *** indicates $p < 0.0005$.

Figure 4. Loss of ketone metabolism in peripheral sensory axons leads to abnormal myelination patterns. (A-B) Representative micrographs of sciatic nerve semi-thin sections stained with toluidine blue used for g-ratio determination (scale bar represents 20 µm). G ratio as determined by myelin and axoplasm area (C) and circumference (D) reveals hypermyelination of small, myelinated axons of the sciatic nerve. Transmission electron micrographs from wildtype (E) and SNACKO (F) mice further revealed myelination errors in SNACKO mice (highlighted by white arrowheads, scale bar represents 5 µm), which are quantified in (G). Additionally, SNACKO mice displayed reduced Remak bundle occupancy compared to wildtype mice (H), indicating both small- and large-fiber deficits in SNACKO mice. (C-D) N-way ANOVA, * indicates effect of genotype: $p < 0.05$, ** indicates effect of genotype: $p < 0.01$. (G-H) Student's t-test, * indicates $p < 0.05$.

Figure 5. SNACKO mice display normal mechano- and thermal-sensation and hyporesponsiveness to intraplantar capsaicin. (A) SNACKO mice exhibited normal

mechanical sensitivity. There was a strong but statistically insignificant trend toward thermal hypersensitivity in SNACKO mice compared to wildtype mice (B). (C) SNACKO and wildtype mice displayed similar sensitivity to cold stimuli as measured by the cold plate test. SNACKO mice engaged in fewer nocifensive events (licking, biting, lifting, etc.) (D) and spent less time engaged in nocifensive behaviors (E) in response to intraplantar capsaicin compared to wildtype mice. (A-B) N-way, mixed models ANOVA. (D-E) N-way ANOVA, * indicates main effect of genotype: $p < 0.05$, ††† indicates main effect of capsaicin: $p < 0.005$, Ψ indicates interaction effect of genotype-capsaicin: $p < 0.05$, ΨΨ indicates interaction effect of genotype-capsaicin: $p < 0.01$.

Figure 6. Loss of neuronal ketone metabolism decreases intraepidermal nerve fiber density. (A) Representative micrographs of intraepidermal nerve fibers (IENFs) stained with post-gene product 9.5 (PGP9.5; red) and tropomyosin-receptor kinase A (TrkA, green) from glabrous skin of the hindpaw from 6-week-old wildtype and SNACKO mice (scale bar represents 50 μm). SNACKO mice had a lower total IENF density compared to wildtype mice (B). SNACKO mice exhibited a decrease in both $TrkA^{+}$, peptidergic IENF density (C) and $TrkA^{-}$, nonpeptidergic IENF density (D). There was a slight but statistically significant increase in nonpeptidergic to peptidergic IENF density ratio in SNACKO mice compared to wildtype mice (E). (F) Representative micrographs of IENFs stained with PGP9.5 (red) and TrkA (green) from the glabrous skin of the hindpaw from 6–7-month-old wildtype, SNACKO, and Synapsin-$1^{+}/^{Cre}$*Oxct1*$^{flox/flox}$ (Syn1-Cre) mice (scale bar represents 100 μm). There was a significant effect of genotype on IENF density for total, peptidergic, and nonpeptidergic fibers (G-I). SNACKO and Syn1-

Cre mice had lower total (G) and peptidergic (H) IENF density than wildtype controls. (I) Only Syn1-Cre mice had significantly reduced nonpeptidergic IENF density compared to wildtype controls in adult mice. (B-E) Student's t-test, * indicates $p < 0.05$, ** indicates $p < 0.01$, *** indicates $p < 0.005$. (G-I) 1-way ANOVA, with a statistically significant effect of genotype in all figures. Tukey's *post hoc* test, * indicates $p < 0.05$ for the comparison indicated by black line, *** indicates $p < 0.005$ for the comparison indicated by black line.

Figure 7. *Oxct1* deficiency results in abnormal peripheral sensory innervation of the spinal dorsal horn. (A) Representative micrographs of lumbar spinal dorsal horns from 6-week-old SNACKO and wildtype mice stained with TrkA (red) and isolectin B4 (IB4, green; scale bar represents 250 µm). There were no differences in the areas of peptidergic (TrkA, B) or nonpeptidergic (IB4, C) innervation of superficial lamina from SNACKO and wildtype mice. The spinal dorsal horn from SNACKO mice did contain more $TrkA^+$ fibers penetrating through the superficial laminae into deeper areas for the spinal dorsal horn (quantified in D; marked by white arrowheads in A). Student's t-test, * indicates $p < 0.05$.

Figure 8. Loss of ketone metabolism in peripheral sensory axons results in proprioceptive deficits. (A) SNACKO mice did not display any differences compared to wildtype mice in latency to fall during the rotarod test. During grid-walk test, SNACKO mice spent significantly less time walking than wildtype mice (B). Additionally, SNACKO

mice exhibited a significant increase in total paw slips normalized to time walking during gridwalk (C). These effects were not limb dependent, as SNACKO mice exhibit more forepaw slips (D) and hindpaw slips (E) normalized to time compared to wildtype mice. N-way ANOVA, *** indicates a significant effect of genotype: $p < 0.005$.

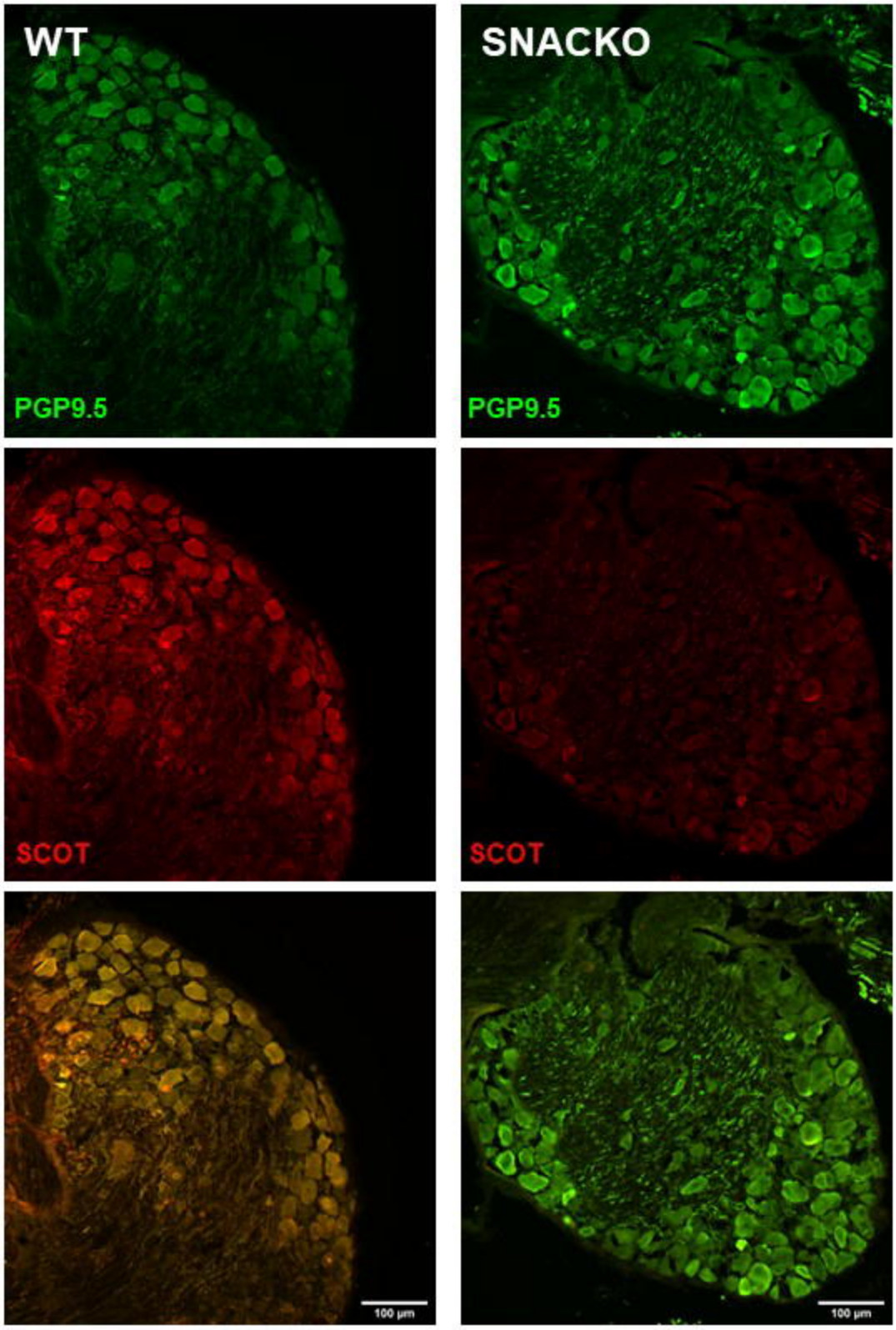
WT
SNACKO
PGP9.5
PGP9.5
SCOT
SCOT
100 µm
100 µm

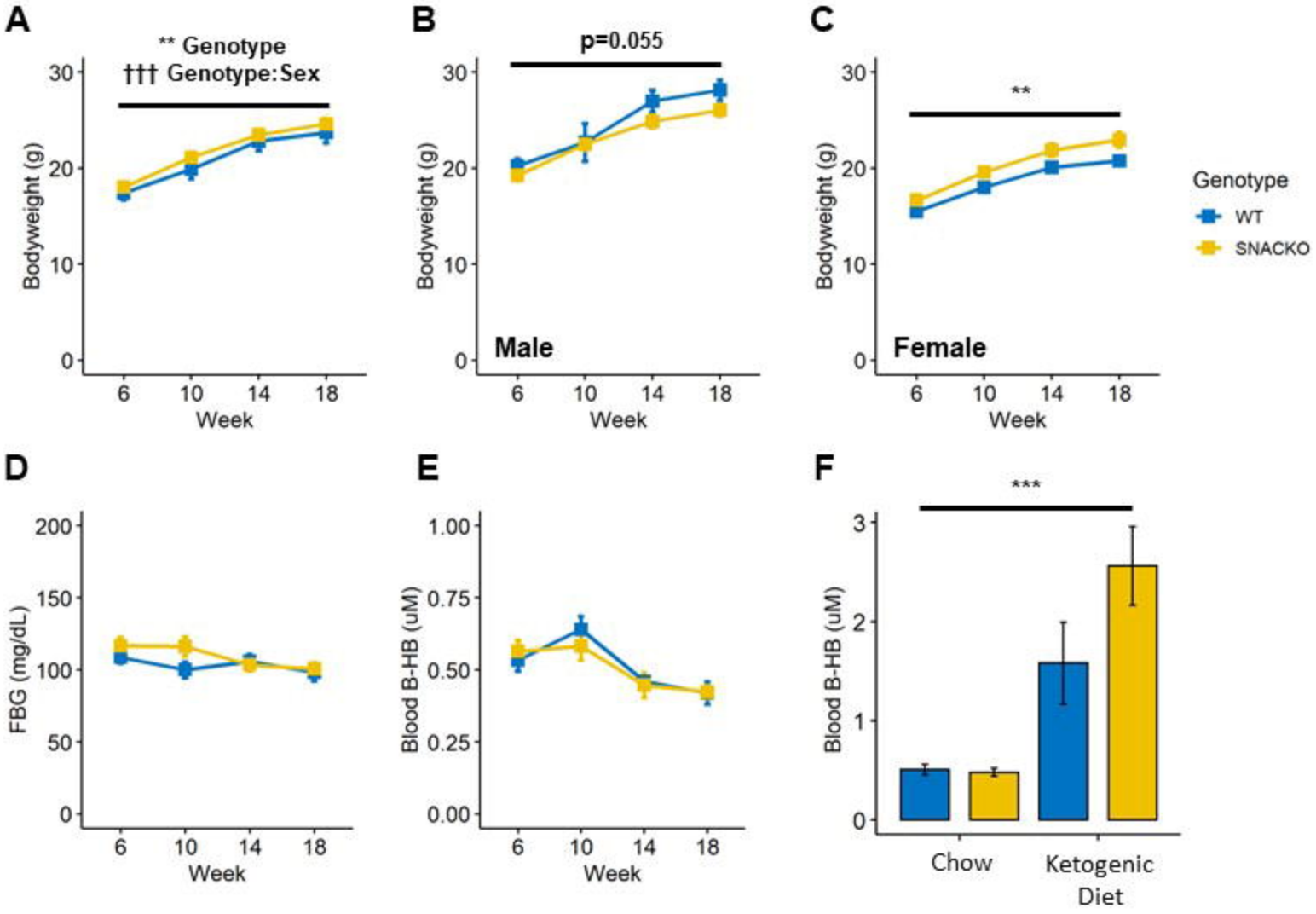
A
** Genotype
††† Genotype:Sex
Bodyweight (g)
Week
B
p=0.055
Male
C
**
Female
Genotype
WT
SNACKO
D
FBG (mg/dL)
E
Blood B-HB (uM)
F
***
Chow
Ketogenic Diet

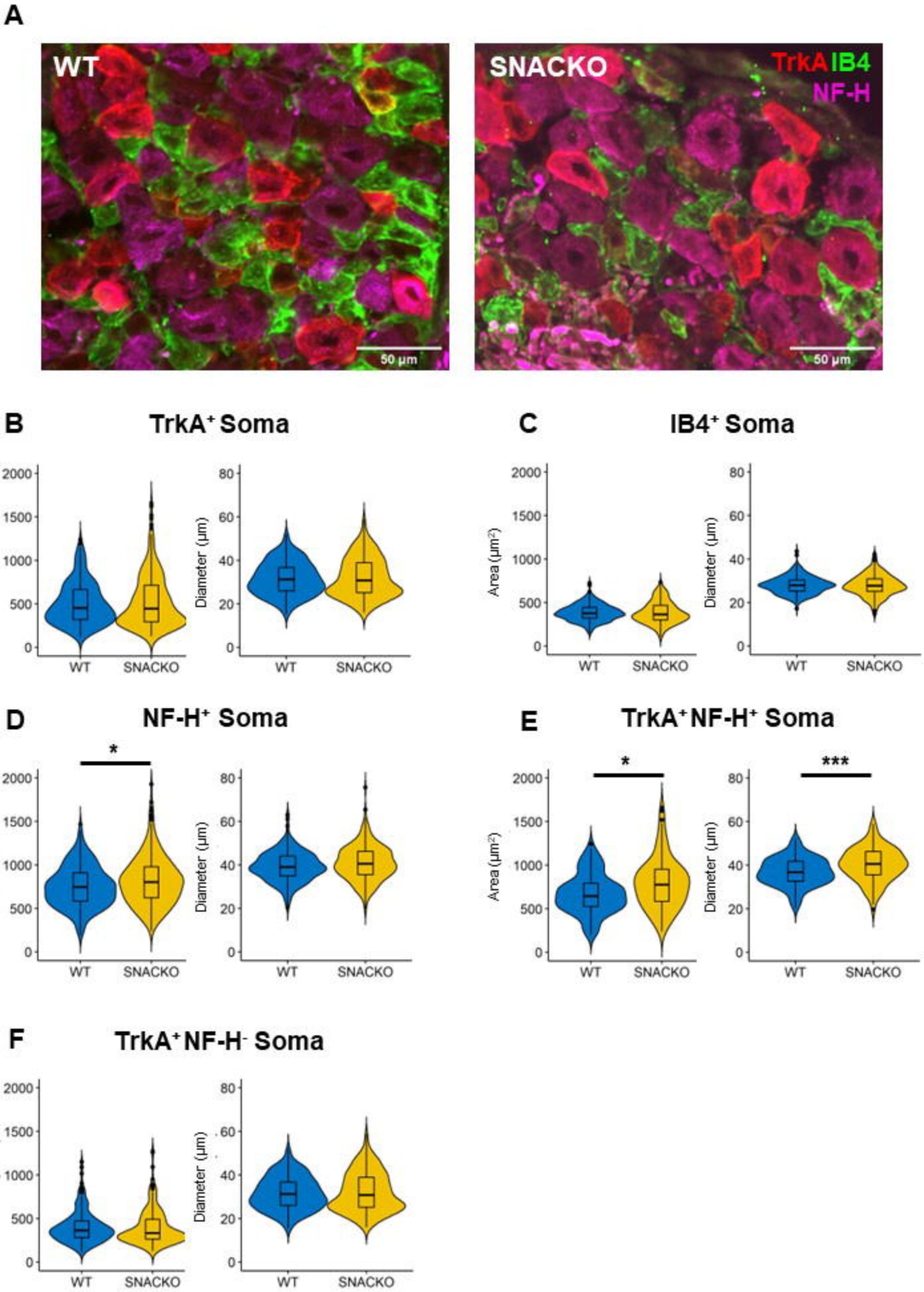
A
WT
SNACKO
TrkA IB4
NF-H
50 µm
50 µm
B
TrkA⁺ Soma
C
IB4⁺ Soma
D
NF-H⁺ Soma
E
TrkA⁺NF-H⁺ Soma
F
TrkA⁺NF-H⁻ Soma
Area (µm²)
Diameter (µm)
WT
SNACKO
*
***

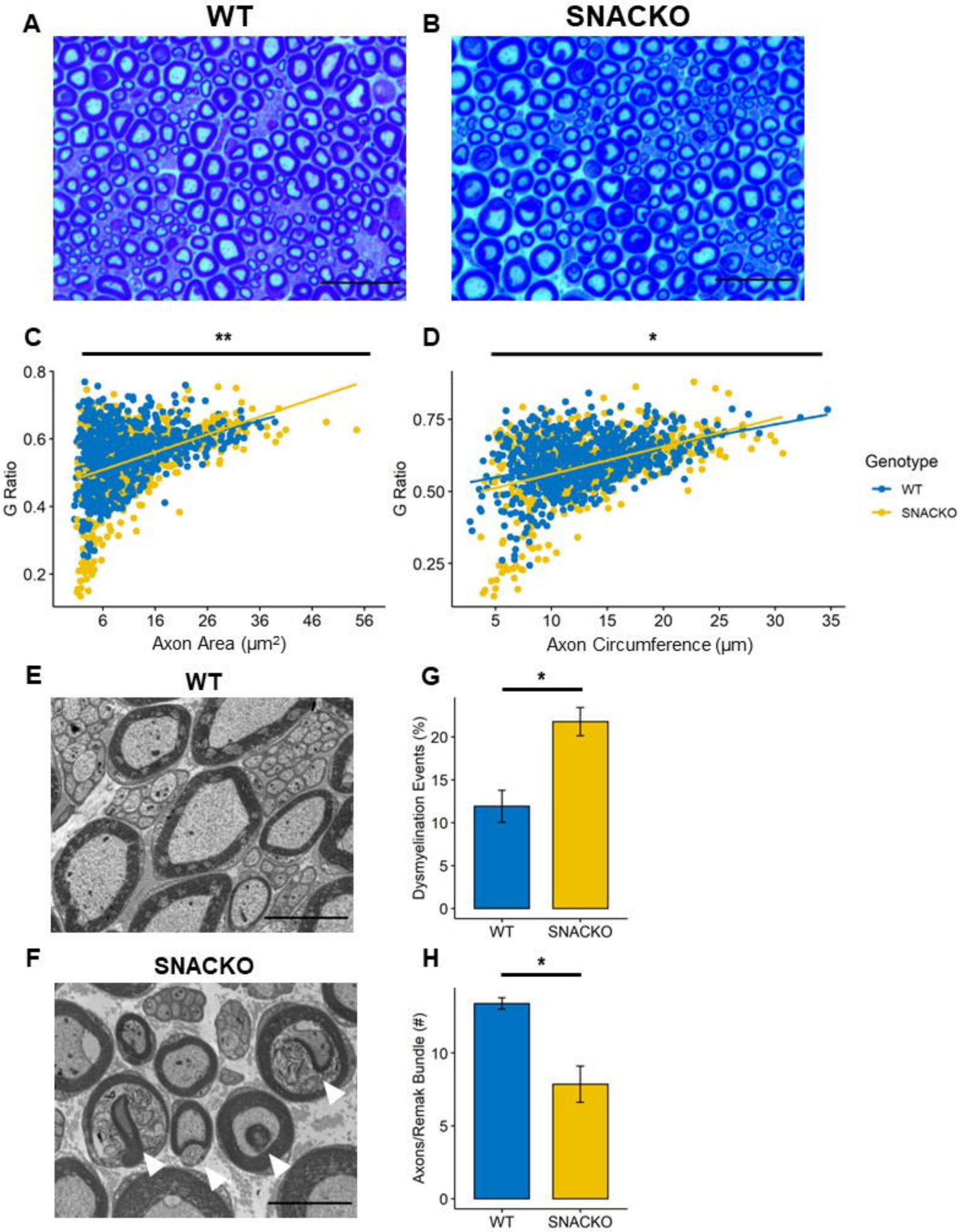
A
WT
B
SNACKO
C
**
G Ratio
0.8
0.6
0.4
0.2
6
16
26
36
46
56
Axon Area (μm²)
D
*
G Ratio
0.75
0.50
0.25
5
10
15
20
25
30
35
Axon Circumference (μm)
Genotype
WT
SNACKO
E
WT
F
SNACKO
G
*
Dysmyelination Events (%)
20
15
10
5
0
WT
SNACKO
H
*
Axons/Remak Bundle (#)
10
5
0
WT
SNACKO

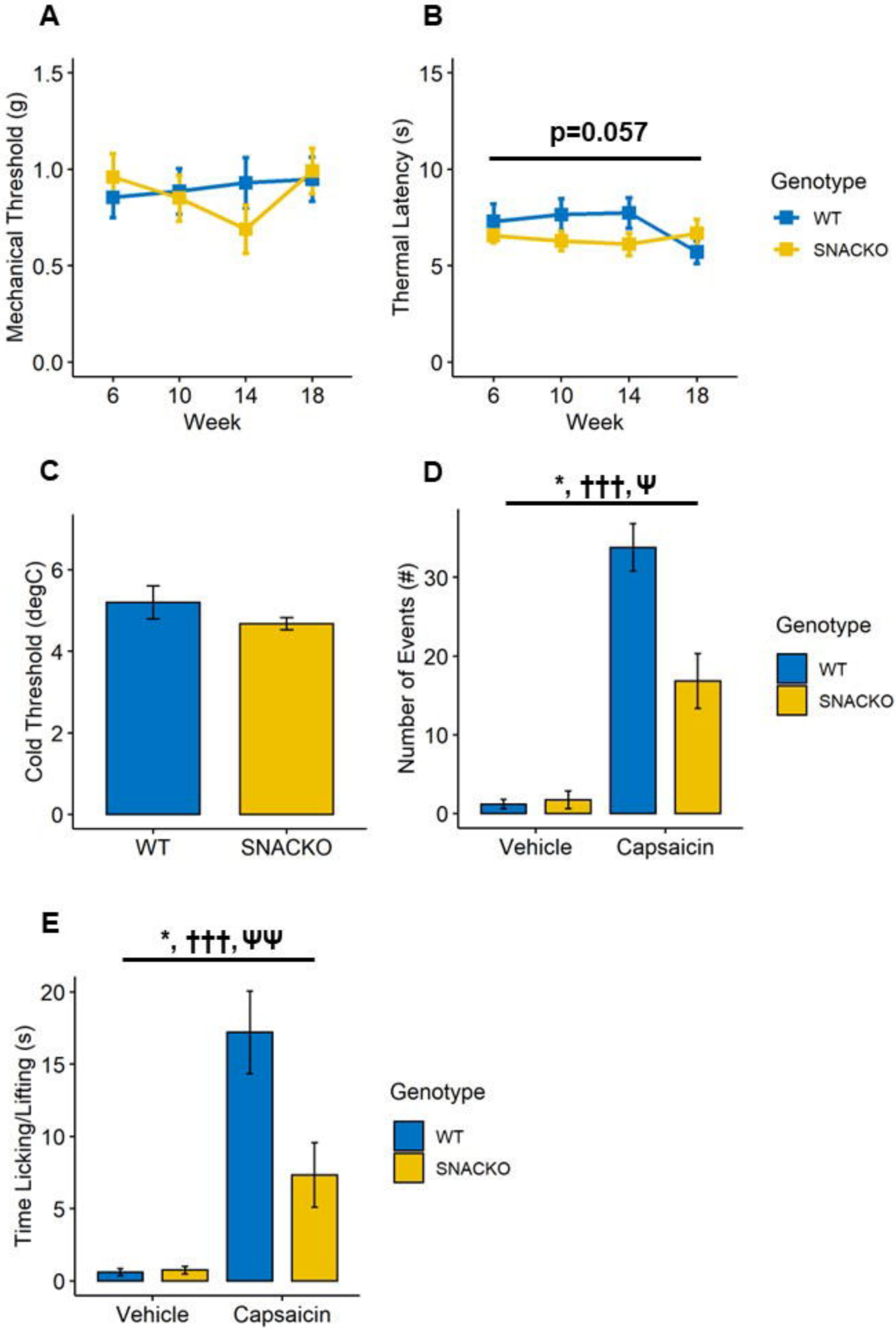
A
Mechanical Threshold (g)
1.5
1.0
0.5
0.0
6
10
14
18
Week
B
Thermal Latency (s)
15
10
5
0
p=0.057
6
10
14
18
Week
Genotype
WT
SNACKO
C
Cold Threshold (degC)
6
4
2
0
WT
SNACKO
D
*, †††, Ψ
Number of Events (#)
30
20
10
0
Vehicle
Capsaicin
Genotype
WT
SNACKO
E
*, †††, ΨΨ
Time Licking/Lifting (s)
20
15
10
5
0
Vehicle
Capsaicin
Genotype
WT
SNACKO

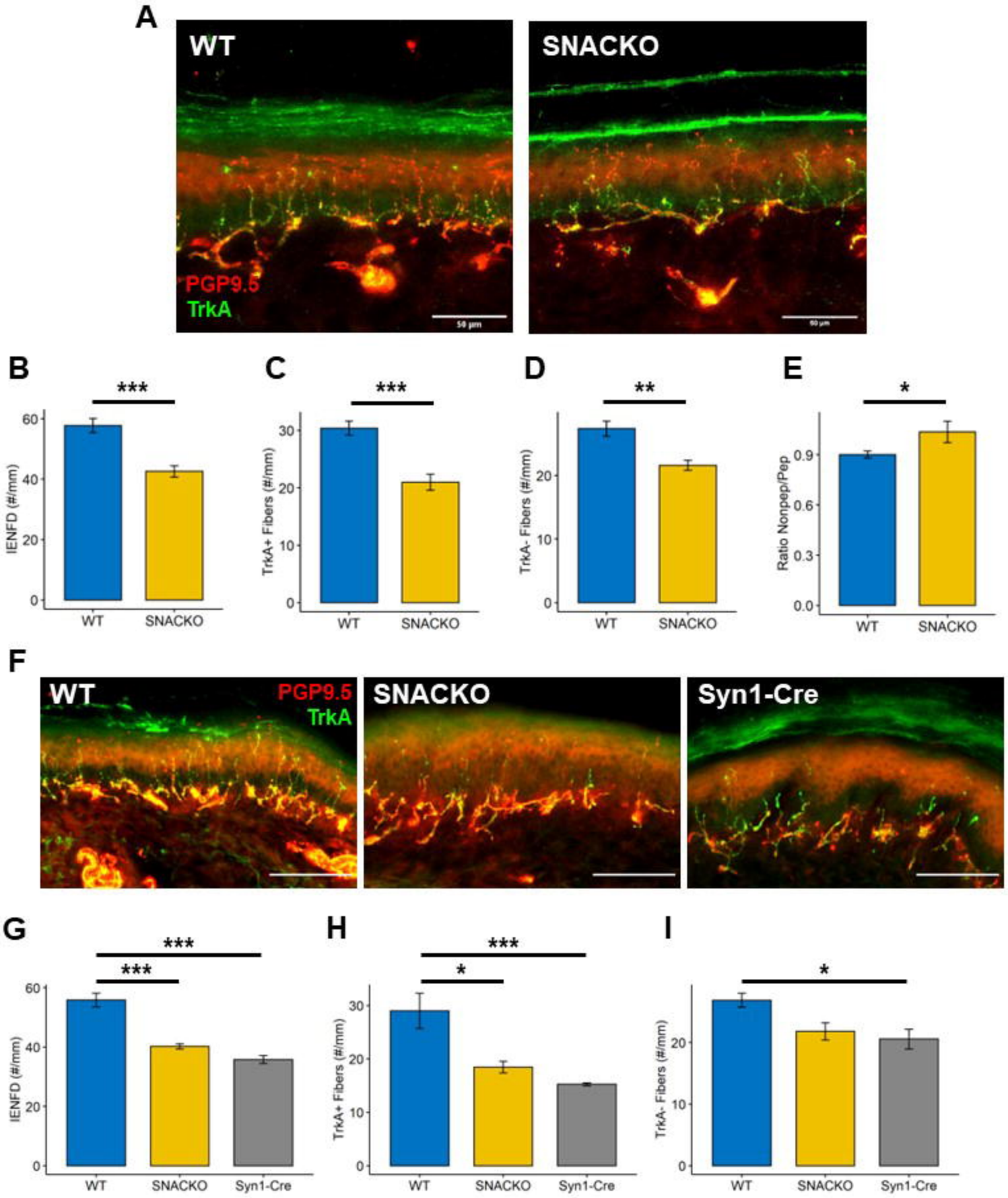
A
WT
SNACKO
PGP9.5
TrkA
B
***
IENFD (#/mm)
WT
SNACKO
C
***
TrkA+ Fibers (#/mm)
WT
SNACKO
D
**
TrkA- Fibers (#/mm)
WT
SNACKO
E
*
Ratio Nonpep/Pep
WT
SNACKO
F
WT
PGP9.5
TrkA
SNACKO
Syn1-Cre
G
***
***
IENFD (#/mm)
WT
SNACKO
Syn1-Cre
H
***
*
TrkA+ Fibers (#/mm)
WT
SNACKO
Syn1-Cre
I
*
TrkA- Fibers (#/mm)
WT
SNACKO
Syn1-Cre

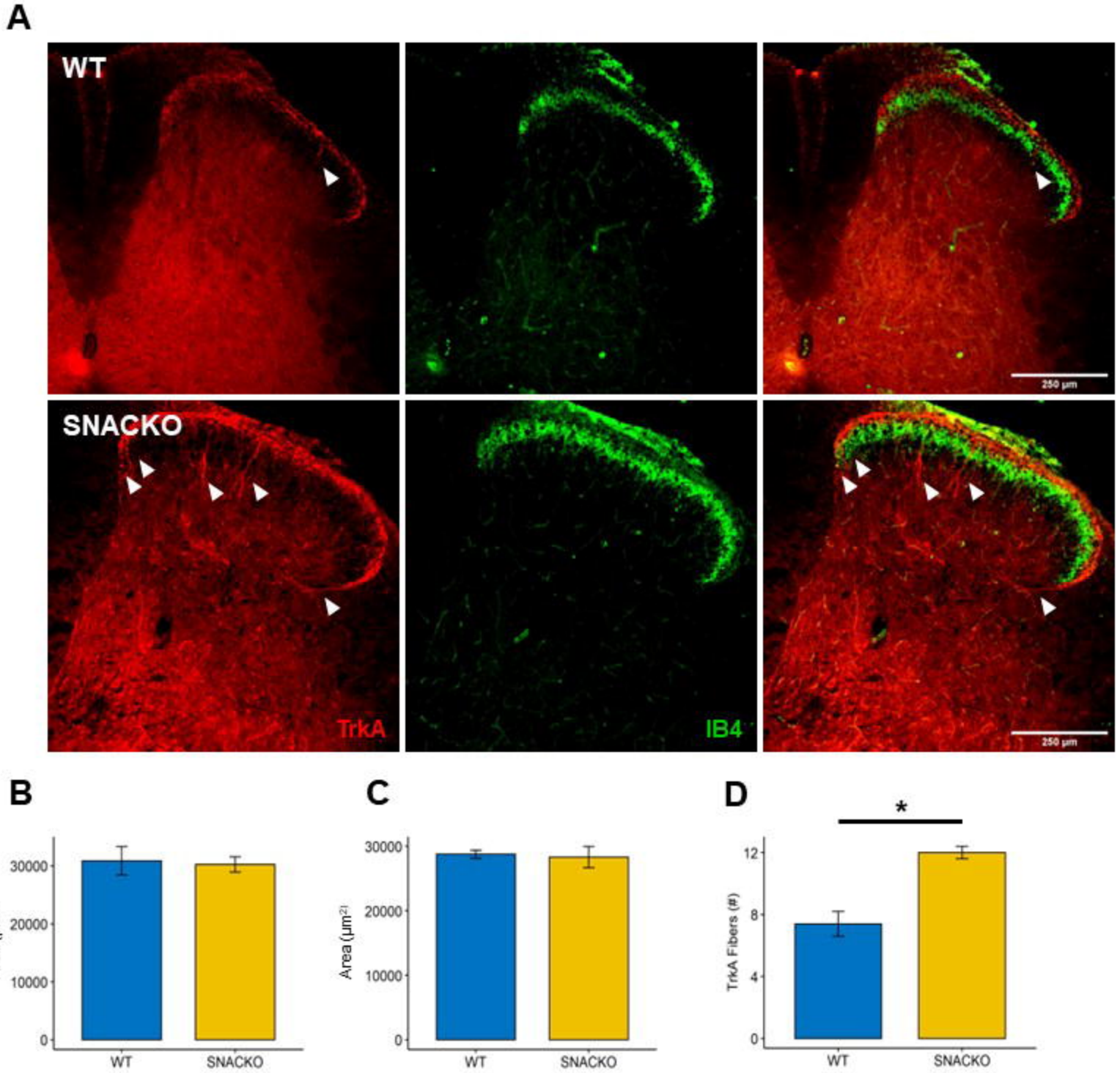
A
WT
SNACKO
TrkA
IB4
250 µm
250 µm
B
Area (µm²)
30000
20000
10000
0
WT
SNACKO
C
Area (µm²)
30000
20000
10000
0
WT
SNACKO
D
*
TrkA Fibers (#)
12
8
4
0
WT
SNACKO

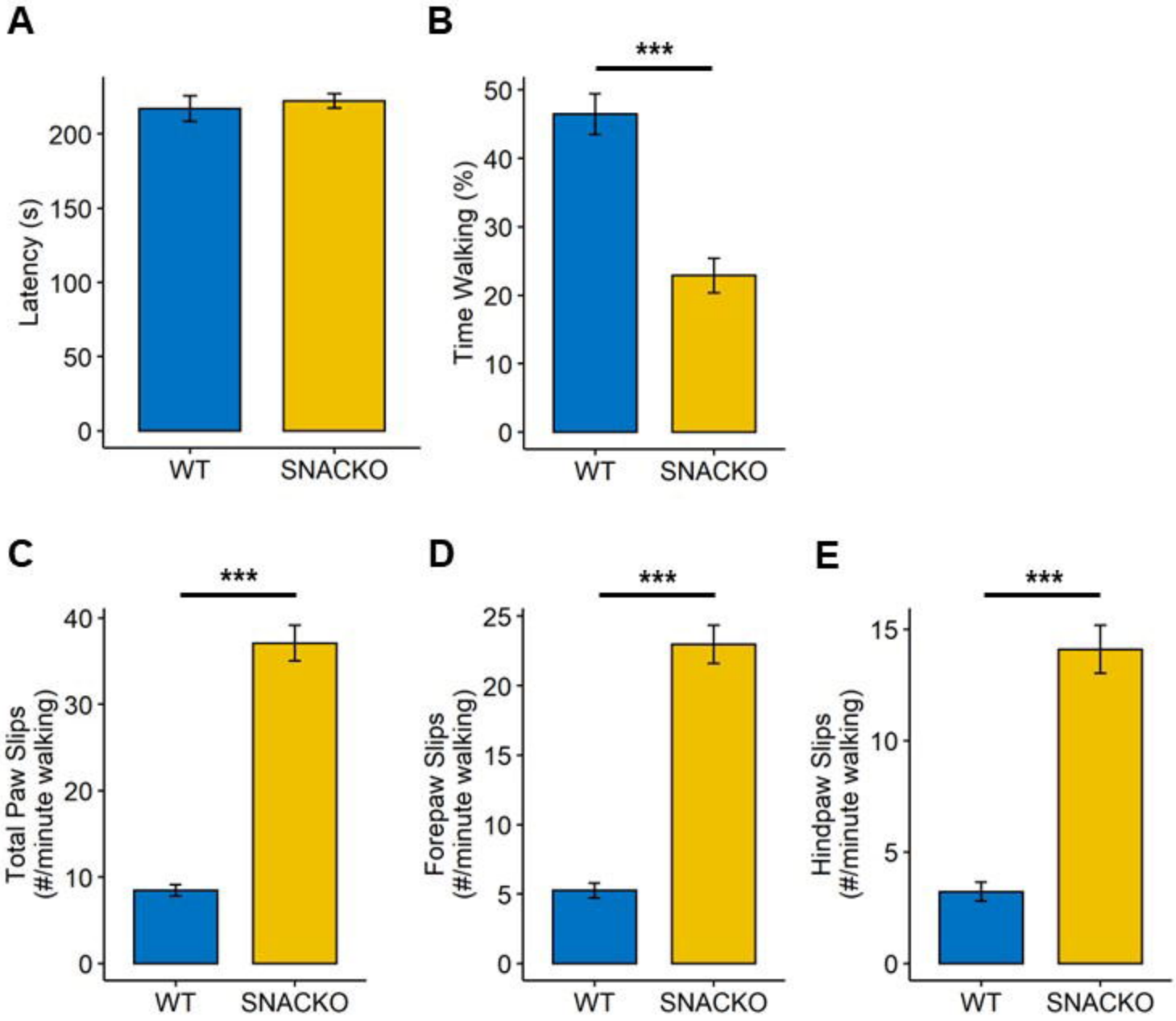
A
Latency (s)
0
50
100
150
200
WT
SNACKO
B
***
Time Walking (%)
0
10
20
30
40
50
WT
SNACKO
C
***
Total Paw Slips
(#/minute walking)
0
10
20
30
40
WT
SNACKO
D
***
Forepaw Slips
(#/minute walking)
0
5
10
15
20
25
WT
SNACKO
E
***
Hindpaw Slips
(#/minute walking)
0
5
10
15
WT
SNACKO